



# HHS Public Access

Author manuscript

*Urolithiasis*. Author manuscript; available in PMC 2020 August 01.

Published in final edited form as:

*Urolithiasis*. 2019 August ; 47(4): 335–346. doi:10.1007/s00240-018-1079-1.

## Development of a Two-Stage Model System to Investigate the Mineralization Mechanisms Involved in Idiopathic Stone Formation: Stage 2- *In Vivo* Studies of Stone Growth on Biomimetic Randall's Plaque

Allison L. O'Kell<sup>1,2</sup>, Archana C. Lovett<sup>3</sup>, Benjamin K. Canales<sup>1</sup>, Laurie B. Gower<sup>3</sup>, and Saeed R. Khan<sup>1,4</sup>

Allison L. O'Kell: aokell@ufl.edu; Archana C. Lovett: arlovett@ufl.edu; Benjamin K. Canales: benjamin.canales@urology.ufl.edu; Laurie B. Gower: lgower@mse.ufl.edu; Saeed R. Khan: khan@pathology.ufl.edu

<sup>1</sup>Department of Urology, College of Medicine University of Florida, 1600 SW Archer Rd, Gainesville, FL, 32610-0247

<sup>2</sup>Department of Small Animal Clinical Sciences, College of Veterinary Medicine, University of Florida, 2015 SW 16<sup>th</sup> Ave, Gainesville, FL 32610-0126

<sup>3</sup>Department of Materials Science and Engineering, University of Florida, 210A Rhines Hall, P.O. Box 116400, Gainesville, FL 32611-6400, USA

<sup>4</sup>Department of Pathology, College of Medicine, University of Florida, JHMHC D6-33C 1600 SW Archer Road, Gainesville, FL 32610, USA

### Abstract

Idiopathic stone formers often form calcium oxalate (CaOx) stones that are attached to calcium phosphate (CaP) deposits in the renal tissue, known as Randall's plaques (RP). Plaques are suggested to originate in the renal tubular basement membrane and spread into the interstitial regions where collagen fibrils and vesicles become mineralized; if the epithelium is breached, the RP becomes overgrown with CaOx upon exposure to urine. We have developed a two stage model system of CaP-CaOx composite stones, consisting of Stage 1) CaP mineralized plaque, followed by Stage 2) CaOx overgrowth into a stone. In our first paper in this series (Stage 1), osteopontin (and polyaspartate) were found to induce a non-classical mineralization of porcine kidney tissues, producing features that resemble RP. For the Stage 2 studies presented here, biomimetic RPs from Stage 1 were implanted into the bladders of rats. Hyperoxaluria was induced with ethylene glycol for comparison to controls (water). After 4 weeks, rats were sacrificed and the implants analyzed using electron microscopy and x-ray microanalyses. Differences in crystal phase and

---

Corresponding authors: Saeed R. Khan, Khan@pathology.ufl.edu, Laurie B. Gower, LGower@mse.ufl.edu.

Allison L. O'Kell (352-294-4471)

Archana C. Lovett (352-219-8513)

Benjamin K. Canales ((352) 265-8240)

Laurie B. Gower (352-846-3336)

Saeed R. Khan (352-294-5593)

Conflict of Interest:

The authors declare that they have no conflict of interest in this work.

Ethical approval:

This article does not contain any studies with human participants performed by any of the authors.

morphologies based upon the macromolecules present in the biomimetic plaques suggest that the plaques have the capacity to modulate the crystallization reactions. As expected, mineral overgrowths on the implants switched from CaP (water) to CaOx (hyperoxaluric). The CaOx crystals were aggregated and mixed with organic material from the biomimetic RP, along with some amorphous and spherulitic CaOx near the “stone” surfaces, which seemed to become compact and organized towards the periphery. This system was successful at inducing “stones” more similar to human idiopathic kidney stones than other published models.

### Keywords

Urolithiasis; Randall’s plaque; Nephrolithiasis; Kidney Stones; Biomimetic Model System; PILP Mineralization

---

### Introduction:

Kidney stones are estimated to affect 8.8% of the United States population [1]. These stones are most commonly composed of calcium oxalate [2] and are idiopathic in nature [3]. Therapies to dissolve calcium oxalate (CaOx) stones medically are not available; thus, if treatment of the stone is required, procedures to fragment and remove the stone are generally necessary [4]. Preventative strategies such as increasing fluid intake, dietary modification, and medications to decrease urinary super-saturation of relevant solutes may decrease the frequency of recurrence [3]. However, these measures do not necessarily address the underlying renal pathology associated with most idiopathic calcium oxalate kidney stones. Additionally, recurrent episodes are prevalent, with 10 year recurrence rates of 30% reported in first time stone formers [5].

Most idiopathic CaOx stones grow attached to Randall’s plaques (RPs), which are regions of subepithelial tissue that have become mineralized with calcium phosphate (CaP) and ultimately become exposed at the renal papillary surfaces [4, 6]. These plaques are believed to originate either in the basement membrane of the loops of Henle [7] or in the walls of the renal papillary vasculature [8], before they then extend into the interstitium. Despite many years of study and multiple resulting theories, the definitive underlying mechanism(s) behind RP formation have not been determined [4, 9, 10]. To study calcium kidney stone disease, various animal models have been used, including rats with exogenously induced hyperoxaluria, genetically manipulated mouse models of hyperoxaluria, Tamm-Horsfall protein (THP) and/or osteopontin knockout mice [11], and Npt2A-co-transporter knockout mice [12]. Rat models with induced hyperoxaluria produce intratubular CaOx crystal deposits [13]. In models without induced hyperoxaluria, THP knockout mice [14] and Npt2A-co-transporter knockout mice [15] form calcium phosphate (CaP) deposits inside tubules and in the renal papillary interstitium, the former located predominantly in the renal papillary area. Similarly, osteopontin knockout and THP/osteopontin double knockout mice develop calcium phosphate deposits in the renal interstitium in the renal papilla [11]. When hyperoxaluria is then induced in THP/osteopontin double knockout mice [11], osteopontin knockout mice [16], or Npt2A-co-transporter knockout mice [12], intratubular calcium oxalate crystals are present. Despite some similarities to the human condition, no animal

model has been identified that mimics the pathology of the human disease. This is likely because CaOx and CaP urinary supersaturation occur in different renal tubular locations, which does not result in growth of CaOx over CaP deposits in animals with experimental induction of hyperoxaluria [13].

An alternative method to study stone kinetics involves the growth of CaOx stones on foreign bodies implanted into bladders of rats [17–19]. An advantage of this model is the ability to grow and study larger stones than would be possible in the rodent renal pelvis. However, these prior studies involved the use of discs made of filter paper [17], plastic [18], zinc or a variety of other materials [19] as a nidus for stone formation, none of which represent a plaque-like matrix as is found in the *in-vivo* situation. To create a more physiologic model, our group has developed “biomimetic Randall’s plaques” (BRPs) consisting of de-cellularized porcine bladder tissue mineralized with calcium phosphate via several methods, including conventional mineralization and mineralization via the polymer-induced liquid-precursor (PILP) process [20]. In the PILP process, mineralization occurs following the formation of a fluidic amorphous precursor that is induced by negatively charged polymers that sequester ions/clusters of calcium salts [21–23]. Gower *et al.* [21], having found that both calcium phosphate [24, 25] and oxalate [26] minerals can be formed via the PILP process *in-vitro*, hypothesized that the calcium phosphate mineralized tissue forming the nidus for CaOx stones may form via such a non-classical mineralization process [23, 26]. Using this process, our group has now created BRPs using de-cellularized porcine kidney tissue as the first stage of a new model system (recently published in *Urolithiasis* (2018) [27]). The resulting kidney tissue contains both renal tubular structures (with exposed basement membranes) and interstitium (with extracellular matrix); thus, these BRPs are considered to represent a more physiologic model for plaque-induced CaOx stone formation. The objective of the second stage of our model system involving these BRPs was to study idiopathic CaOx stone formation *in-vivo* by implanting BRPs into the bladders of hyperoxaluric rats. We hypothesized that hyperoxaluric rats would form CaOx overgrowths on the implanted BRPs that were morphologically similar to native idiopathic CaOx stones, but there might be differences between BRPs produced via the PILP process versus the conventional mineralization process.

## Materials and Methods:

### Preparation of implants.

The BRP implants were constructed using porcine kidney tissue de-cellularized as described elsewhere [28], approved by the University of Florida’s Institutional Animal Care and Use Committee (study 201307895). To form the BRPs, the kidneys were cut into 10 mm × 5 mm sections and placed in the corresponding mineralization solutions to generate the following 3 types of BRPs: 1) tissue mineralized with calcium phosphate alone (conventional mineralization); 2) PILP-mineralization of calcium phosphate with poly-L-aspartic acid (polyAsp); or 3) PILP-mineralization of calcium phosphate with osteopontin (OPN). The latter two used the polypeptide or protein, respectively, as process-directing agents to induce the PILP process, as described in detail in our companion paper for Stage 1 [27].

Samples from each of the above conditions, plus non-mineralized tissue (control), for bladder implantation were placed in sterile vials and 70% ethanol was added for 20 minutes. The samples were rinsed with sterile saline three times, then stored in a fresh sterile vial with sterile saline until implantation.

### **Animals.**

Thirty two 4-week old male Sprague Dawley rats were used in this stage 2 study. Rats were paired in cages and provided a free choice standard rodent diet with free choice water for 1 week prior to surgery. The animal protocol was approved by the University of Florida's Institutional Animal Care and Use Committee (study 201107167).

### **Implantations.**

Rat pairs were randomly assigned to receive either regular water (n =16) or water containing 0.75% ethylene glycol (EG) (n=16). Each group was then randomly assigned to one of the following four bladder implant groups: (a) control (decellularized non-mineralized renal tissue) (DNM control group), (b) conventionally-mineralized BRP implant (BRP-C group), (c) PILP mineralization with poly-Asp (BRP-PA group), and (d) PILP mineralization with OPN (BRP-OPN group). Each experimental group contained 4 rats.

Surgical implantation of the kidney tissues into the bladder of the rats was carried out under isoflurane anesthesia in a designated surgical suite. Each rat was prepped for abdominal surgery [hair clipped, skin sterilized] then covered with a sterile disposable surgical drape. An incision was made with a scalpel in the caudal abdomen and the bladder was exposed. Stay sutures were placed to maintain bladder positioning. The cranial bladder was incised and the implant was sutured to the internal bladder wall at the apex. Each implant was approximately 0.5 cm in length. The bladder incision and muscular layer of the abdomen were then closed using sterile absorbable sutures and the skin was closed using surgical clips.

Rats were given 0.05 mg/kg buprenorphine subcutaneously prior to the first incision and every 12 h thereafter for 48 h. Following recovery from anesthesia, rats were immediately allowed access to food and water. The EG-treated rats received regular water for 4 days post-operatively during recovery, then placed on EG-containing water again on Day 5 post-operatively. Surgical clips were removed 10–14 days post-operatively under isoflurane anesthesia.

### **Post-implantation procedures.**

Rats were maintained in pairs in standard cages for 4 weeks. On days 7, 14, and 21, post-operatively rats were placed in metabolic cages for collection of three hour urine samples for measurement of pH (using test strips) and microscopic examination. Crystals were filtered and collected from select urine samples to be examined with scanning electron microscopy (SEM) for additional crystal morphological analysis. On days 7 and 21, rats remained in the metabolic cages for 24 hour urine collection for determination of oxalate and calcium excretion. After the 3 hour samples were collected on these days, 1 ml 1N HCl was placed

into urine collection tubes of metabolic cages to adjust  $\text{PH} < 7$ . After 24 hour urine collections, sodium azide was added into the urine up to final concentration was 0.02%.

Rats were sacrificed 4 weeks after surgery. Kidney sections and whole bladders (including bladder implants) were placed into separate formalin containers for evaluation by light microscopy and scanning electron microscopy with energy dispersive spectroscopy (EDS) to identify the crystals [29]. The bladder implants were first scanned with  $\text{Cu-K}\alpha$  X-ray radiation from a PANalytical X’Pert Pro Powder Diffractometer at 45 kV and 40 mA, using a step size of  $0.01^\circ\text{mrad s}^{-1}$  over a  $2\Theta$  range of  $10\text{--}70^\circ$ . Next, they were mounted on SEM stubs and coated with carbon for analysis using a JEOL 6400 SEM or and FEI XL-40 FEG SEM.

### Urinary oxalate and calcium measurements.

Urinary oxalate measurements were performed using the Oxalate Determination Kit (Trinity Biotech Cat#: 591D). Additional urine was stored at  $-80$  Celsius, and urine calcium was determined a later time point using modification of the calcium o-cresophthalein complexone reaction with a Dimension clinical chemistry system (Siemens, USA).

## Results:

### Urinary oxalate and calcium excretion.

All rats survived the surgical procedures, as well as the 4 week post-surgical study period without complications. Twenty-four hour urinary oxalate levels measured on day 7 (data not shown) and day 21 (Fig. 1) were higher in all EG-treated rats compared to rats placed on regular water. Urinary calcium excretions were below the limit of detection in the EG-treated rats ( $< 5$  mg/dL) in 15/16 rats on day 7 and 16/16 on day 21. For rats receiving regular water, the mean 24 hour urinary calcium levels on day 7 was  $1.3 \pm 0.45$  mg/day for 12/16 rats having detectable levels, but by day 21 the urinary calcium levels were undetectable in 13/16 rats.

### Urinary pH and microscopy.

Median urine pH was lower in EG rats at day 7 (median = 7.25; range = 6–8.5), day 14 (median = 6; range = 5–7.5), and day 21 (median = 6.5; range = 5–7.5) compared to regular water rats at day 7 (median = 8.5; range = 7.5–8.5), day 14 (median = 8; range = 7–8.5) and day 21 (median = 8.25; range = 6.5–8.5). With respect to urine crystals, 15/16 regular water rats had struvite crystals detected via light microscopy at one or more time points, and 7/16 EG rats had  $\text{CaOx}$  dihydrate crystals detected at one or more time points. Rat urine samples were also dried and examined with SEM, and representative images of the urinary crystals are shown in Fig. 2. In general, rats receiving regular water had predominantly struvite type crystals (both the ammonium and potassium magnesium phosphate forms along [30, 31]), with some calcium phosphate, while rats receiving ethylene glycol had  $\text{CaOx}$  mono- and dihydrate crystals. Agglomerates of non-faceted mineral particles which were likely amorphous were also common in all groups. The submicron particles in Fig. 2a and many other images appear to be partially coalesced. Many of the large phosphate crystals appear to have a coating made up of similarly sized particles (Fig. 2a & b), suggesting they may have

formed from attachment and partial coalescence of amorphous colloids. Although the attached particles are mostly non-descript in shape (and could be construed as being organic in nature), some can be seen as having edges that align with the crystal facets (and thus crystal planes) of the underlying crystal, and thus are likely amorphous mineral particles undergoing iso-epitaxial crystallization with the underlying crystalline substrate upon which they had deposited. The samples were not thoroughly rinsed before drying, so these small deposits may have simply formed during the rapid rise in supersaturation upon drying.

### Morphological analysis of implants.

During tissue collection post-mortem, all rats were found to have implants remaining in their bladders (Fig. 3). SEM of each implant revealed mineralization in all specimens analyzed, but with considerably less in the DNM samples that did not originally contain CaP mineral (although this was variable). In some cases, there was no visual evidence of crystals, yet EDS showed the presence of a small amount of Mg and P (Fig. 4a,b). Overall, rats consuming regular water formed mostly magnesium phosphate or calcium phosphate crystals on the implants, with a broad range of sizes and morphologies (Figs. 4 & 5). Interestingly, while most of the urine crystals appeared to be struvite, the crystals in the stones did not exhibit the struvite morphologies, nor did they show a nitrogen peak in the EDS spectrum. X-ray diffraction of the crystals shown in Fig. 4c,d showed patterns consistent with the brushite (dicalcium phosphate dihydrate) phase, while those from Fig. 5b & d were difficult to identify, but appear to be some form of magnesium-calcium-dihydrogen phosphate phase (Fig. S1). Fibrous segments of the BRPs are visible in some areas intermixed with crystals (Fig. 4b and 5a). The densely packed, aligned fibers seen in Fig. 5b might correspond to elastin fibers that were seen via TEM in the BRPs examined in our Stage 1 report [27].

In contrast, the implants from EG-treated rats formed mostly CaOx stones on all the implants (Figs. 6 & 7). The overgrowths were so extensive that the original BRP tissue was less easily discerned; but in some areas near the interiors of the stones, the crystals were more isolated and intermingled with the decellularized kidney tissue (Figs. 6c, 7 b,c). Organic matter was also seen covering the surface of most of the stones, and could also be seen in smaller quantities intermingled with the CaOx crystal overgrowths throughout the body of the stones. It did not appear to be from the original BRP implant because it contained small lumps or nodules along fibrous material which had not been seen in the original BRP (Supplementary Material Figs. S2 – S5); therefore, we believe this organic material accumulated from the urine and deposited onto the forming stone, possibly in a hydrogel form (Supplementary Material Fig. S4).

The surface of the stones formed on DNM implants (Fig. 6a) showed the tips and edges of tightly packed aggregates of CaOx monohydrate (COM) crystals. Individual COM crystals appeared as thin plates and were scattered on the surface as well as inside the stones (Fig. 6b). Those with the typical “coffin” shaped morphology of COM appeared to collect in a random fashion; but in some regions, they were tightly packed into stacks of tablets that seemed to terminate in an overall spherical aggregate (Fig. 6a). Interpenetrant twinning of COM crystals was occasionally seen (Fig. 6b). Stones formed on BRP-C implants (Fig. 6



c,d) were similar in appearance to those formed on the DNM implants on the interior, consisting of a random collection of “coffin” shaped COM crystals which were often twinned (Fig. 6c). A fracture surface (Fig. 6d) shows a radial arrangement of thin rod or needle-like crystals that is more clearly representative of a spherulitic type of growth pattern, and which even exhibited a concentric-layered growths.

Stones formed on the BRPs prepared with the process-directing additives (Fig. 7) contained less of the loose and random aggregates of COM “coffins”, and instead the COM appeared mostly in the form of dumbbells or rosettes of stacked plates interrupted by interpenetrant twinned crystals. Stones grown on BRP-PA contained both COM and COD crystals (Fig. 7a). The COD crystals were relatively sparse and had the distinct tetragonal bipyramidal shape. A meshwork of BRP tissue fibers can often be observed towards the center of the stones (Fig. 7b). Moving towards the periphery, COM crystals are visible individually and as stacked structures, but then seem to become very compact at the surface. Although the stones developed on BRP-OPN contained mostly COM crystals, the stone surface showed a highly organized and compact morphology with radially arranged COM crystal plates in some regions (Fig. 7c). Internally, the COM crystals were generally aggregated dumbbells, but with strikingly thick layers (Fig. 7d).

## Discussion:

In this study, BRPs were successfully implanted into the bladders of normal or hyperoxaluric rats, leading to the formation of an implant associated stone. All rats that received ethylene glycol had higher urinary oxalate excretions than rats receiving regular water, excreted CaOx crystals in the urine, and formed CaOx stones on the implanted BRPs. Rats receiving regular water excreted calcium phosphate and struvite like crystals, and developed structures resembling struvite stones containing calcium phosphate and/or magnesium and phosphate, which is consistent with previous studies of foreign body stones in rats [18, 19]. Calcium phosphate crystals have also been previously noted in the urine of healthy control rats [32, 33], so the calcium phosphate components to the stones of some control rats is not overall surprising and may be partially due to alkaline urine in control rats [34, 35]. We have previously shown that urine of male Sprague-Dawley rats is supersaturated with respect to struvite and often contained struvite crystals [18]. Ethylene glycol administration led to elevation of urinary oxalate and CaOx supersaturation and induction of CaOx crystalluria [18]. Implantation of foreign bodies (comprised of plastic) in their urinary bladder and changing urinary conditions by administering ethylene glycol for two weeks at 2 week intervals led to the deposition of alternating layers of CaOx and mixture of calcium phosphate and struvite [18]. Similar to the present study, urinary pH was lower when rats were on ethylene glycol.

In the present study, hyperoxaluric rats mostly excreted urine with COM crystals and COM crystals were the predominant phase deposited on the implanted BRPs. Even the non-mineralized kidney tissue caused pronounced overgrowth with CaOx crystals, and in a morphological structure which resembles stones. This seems to suggest the CaP mineral component of RP is not a necessary ingredient for stimulating stone formation in this *in-vivo* study. However, these conditions were quite extreme, so the influence of the underlying

mineral in plaque could be overwhelmed from this high level of oxaluria. While it is difficult to compare oxalate excretion in rats to humans due to difference in body size, hyperoxaluria in humans is defined as excretion of greater than 45 mg/day [36], which is approximately 0.69 mg/kg/day based on an average 65 kg human. At day 21, our rats were excreting approximately 9 mg/day, which is 69 mg/kg/day based on approximate weight of 0.13 kg per rat, and is approximately 100 fold higher than the definition for hyperoxaluria in humans. High urinary oxalate to calcium ratio generally leads to CaOx monohydrate crystals [37], and is likely also the case in this study given the high oxalate excretion and undetectable urine calcium in most rats in the EG groups. The presence of COD crystals in association with the BRP’s made in the presence of poly-L-aspartic acid may indicate its role in inhibiting the monohydrate phase (*i.e.*, stabilizing the COD phase). Consistent with our findings, poly-L-aspartic acid has been shown by others to favor crystallization of COD over COM *in-vitro* [38]. In some cases, pits could be seen in the COD crystals; these were likely undergoing dissolution-reprecipitation to the more stable COM phase which could be seen as small plates growing off the neighboring surfaces (Supplementary Material Fig. S6).

In nearly all the samples analyzed, there was a consistent trend in the morphological analyses, with the interior of the stones showing a loose aggregation of CaOx crystals mixed with BRP organic material and presumably CaP (although CaP crystals were rarely seen), which then transitioned into the CaOx mineral becoming more compact and organized towards the periphery of the “stone”. This is most apparent in Fig. 7b & d, which shows a condensed stone-like morphology (other examples are shown in Supplementary Material Fig. S2–4). Similar crystal morphologies, including stacked COM plates, have been found at the interface between Randall’s plaque and the calcium oxalate stone from human patients examined via SEM [39]. Interestingly, they observed stacked plate aggregates that transitioned into thinner plates (with needle-like subunits); a similar transition was observed in our “biomimetic stones” (Supplementary Material Fig. S3, S7, S8). These then transitioned into fine dendritic structures, which we did not see. They attribute the morphological changes to variations in urinary supersaturation. This seems less likely in our bladder model, so we offer an alternative explanation for this sequence of morphological changes. Based on our overall observations from all of the “biomimetic stones”, the BRP matrix clearly provided a favorable substrate for heterogeneous nucleation of CaOx (with or without CaP), which initially occurred as a random assortment of isolated plates (coffins), but these crystals then provided an even more favorable substrate for secondary nucleation and/or twinning (Supplementary Material Fig. S8) to create the more densely packed layered dumbbells or rosettes (Supplementary Material Fig. S9). These regions then seemed to stimulate radial outgrowths into the more densely-packed conventional spherulites (Supplementary Material Fig. S3 & S7). In some cases, an amorphous granular substance could be seen in the transition region to radial outgrowths. One can’t tell from the images if it is amorphous mineral or organic material, but the granular phase appears to be fusing into the growing crystals (Supplementary Material Fig. S7). Spherulitic textures do not necessarily have to grow from an amorphous phase, but can also arise from a high density of nucleation sites (or twinning). Therefore, the edges of a favorably oriented COM platelet could conceivably lead to iso-epitaxial nucleation of multiple crystallites, which if oriented along the rapid growth direction could then dominate the subsequent growth and develop



into the new texture (Supplementary Material Fig. S8). Alternatively, some later deposited organic matrix could provide a high density of nucleation sites. Supplementary Material Fig. S2 shows a dense coverage of nodular organic matrix which appears to accumulate on the surface of the “stones”. The same fibrous mesh was often seen to be intimately associated with the CaOx aggregates within the interior of the stones, and even became enmeshed within the layered aggregates (Supplementary Material Fig. S5). We suspect this organic matrix plays a decisive role in the unusual morphological development of the stacked plate COM aggregates and rosettes (Supplementary Material Fig. S5 & S9). The subjectively greater amount of organic material observed on the implants of the EG group rats could be potentially stem from inflammation in the kidney, secondary to crystal induced damage. Crystal induced renal injury and/or inflammation has been documented with multiple different crystal types in both animal models and humans [40].

The outer surfaces of the BRP associated stones appeared nodular with radially and concentrically organized COM crystals. This morphology is reminiscent of human CaOx monohydrate kidney stones, which have a disorganized core comprised of crystals or calcified tubules, and a highly structured outer zone of radially striated and concentrically laminated CaOx monohydrate [4, 41, 42]. Although human stones are often more dense in the interior, our BRP implants are relatively large with respect to the CaOx overgrowths formed over them, so it is not surprising that we observe more of the loose interior. Also, during idiopathic stone formation, much smaller pieces of native RP may be exposed in the renal pelvis that could stimulate overgrowths, and over the long duration of stone formation, they would appear to be a minor constituent of the overall composite stone.

This study has a number of limitations. Conditions in the urinary bladder may not be the same as in the kidney; however, placement of implants in bladders is much more feasible than into the rat kidney. BRPs were studied at only one time point, and were continuously bathed in highly hyperoxaluric urine, which does not reproduce idiopathic stone former conditions in humans but is the only way to induce the similar two-stage composite stones in a rat model. Lastly, the conditions of hyperoxaluria were so extreme that subtle differences between the BRPs influence on promoting crystal nucleation and growth might not have been resolved. Such differences may be particularly relevant to the human system of idiopathic stone formation which is not at such a high CaOx supersaturation.

## Conclusions:

In summary, results of this study indicate that exposure of a CaP mineralized kidney tissue substrate to hyperoxaluric conditions can lead to the development of a CaOx composite stone similar in morphology to human idiopathic calcium oxalate stones. Even without conditions of hyperoxaluria, calcium phosphate stones could also be produced, particularly when the BRP matrix already contained CaP mineral. Differences in crystal phase and morphology based upon the macromolecules present in the plaque suggest that the plaque has the capacity to modulate the crystallization pathways, which might be more pronounced under more moderate levels of hyperoxaluria. In the future, it would be interesting to perform a kinetics study under conditions with less extreme hyperoxaluria by administering 0.5% EG solution, and examine the implants at 3 days, one week, 2 weeks and 4 weeks to

study progress of stone development. Although the differences between the different groups of BRP-induced stones were relatively minor, close morphological analyses suggest that accumulation of organic matter might play an influential role in the stone formation mechanism(s), and therefore may be an area to target future development of therapeutic agents. Future studies may also include evaluating the effects of administering other stone-associated proteins (*e.g.*, Tamm-Horsfall glycoprotein) or other compounds (citrate, Mg-ion, *etc.*), on stone growth and morphology.

## Supplementary Material

Refer to Web version on PubMed Central for supplementary material.

## Acknowledgements:

Research reported in this publication was supported by the National Institute of Diabetes and Digestive and Kidney Diseases of the National Institutes of Health under Award Number R01DK092311. The content is solely the responsibility of the authors and does not necessarily represent the official views of the National Institutes of Health. We also thank our collaborators who provided the decellularized porcine kidney tissues, Drs. Brad Willenberg and Edward Ross (College of Medicine, University of Central Florida), and Dr. Christopher Batich (Department of Materials Science and Engineering, University of Florida). Data was also gathered from EM core in the College of Medicine, as well as the Research Service Centers within the Herbert Wertheim College of Engineering, so we thank the staff for their training and guidance on these instruments as well.

## References:

- [1]. Scales CD, Smith AC, Hanley JM, Saigal CS, Project UDiA (2012) Prevalence of kidney stones in the United States. *Eur Urol* 62: 160–165 [PubMed: 22498635]
- [2]. Lieske JC, Rule AD, Krambeck AE, et al. (2014) Stone composition as a function of age and sex. *Clin J Am Soc Nephrol* 9: 2141–2146 [PubMed: 25278549]
- [3]. Worcester EM, Coe FL (2010) Clinical practice. Calcium kidney stones. *N Engl J Med* 363: 954–963 [PubMed: 20818905]
- [4]. Khan SR, Pearle MS, Robertson WG, et al. (2016) Kidney stones. *Nature reviews Disease primers* 2: 16008
- [5]. Singh P, Enders FT, Vaughan LE, et al. (2015) Stone Composition Among First-Time Symptomatic Kidney Stone Formers in the Community. *Mayo Clin Proc* 90: 1356–1365 [PubMed: 26349951]
- [6]. Evan AP, Worcester EM, Coe FL, Williams J, Lingeman JE (2015) Mechanisms of human kidney stone formation. *Urolithiasis* 43 Suppl 1: 19–32 [PubMed: 25108546]
- [7]. Evan AP, Lingeman JE, Coe FL, et al. (2003) Randall’s plaque of patients with nephrolithiasis begins in basement membranes of thin loops of Henle. *J Clin Invest* 111: 607–616 [PubMed: 12618515]
- [8]. Stoller ML, Meng MV, Abrahams HM, Kane JP (2004) The primary stone event: a new hypothesis involving a vascular etiology. *J Urol* 171: 1920–1924 [PubMed: 15076312]
- [9]. Bird VY, Khan SR (2017) How do stones form? Is unification of theories on stone formation possible? *Arch Esp Urol* 70: 12–27 [PubMed: 28221139]
- [10]. Hsi RS, Ramaswamy K, Ho SP, Stoller ML (2017) The origins of urinary stone disease: upstream mineral formations initiate downstream Randall’s plaque. *BJU Int* 119: 177–184 [PubMed: 27306864]
- [11]. Mo L, Liaw L, Evan AP, Sommer AJ, Lieske JC, Wu XR (2007) Renal calcinosis and stone formation in mice lacking osteopontin, Tamm-Horsfall protein, or both. *Am J Physiol Renal Physiol* 293: F1935–1943 [PubMed: 17898038]

- [12]. Khan SR, Glenton PA (2008) Calcium oxalate crystal deposition in kidneys of hypercalciuric mice with disrupted type IIa sodium-phosphate cotransporter. *Am J Physiol Renal Physiol* 294: F1109–1115 [PubMed: 18337544]
- [13]. Khan SR (2010) Nephrocalcinosis in animal models with and without stones. *Urol Res* 38: 429–438 [PubMed: 20658131]
- [14]. Liu Y, Mo L, Goldfarb DS, et al. (2010) Progressive renal papillary calcification and ureteral stone formation in mice deficient for Tamm-Horsfall protein. *Am J Physiol Renal Physiol* 299: F469–478 [PubMed: 20591941]
- [15]. Khan SR, Canales BK (2011) Ultrastructural investigation of crystal deposits in Npt2a knockout mice: are they similar to human Randall’s plaques? *J Urol* 186: 1107–1113 [PubMed: 21784483]
- [16]. Wesson JA, Johnson RJ, Mazzali M, et al. (2003) Osteopontin is a critical inhibitor of calcium oxalate crystal formation and retention in renal tubules. *J Am Soc Nephrol* 14: 139–147 [PubMed: 12506146]
- [17]. Khan SR, Hackett RL (1985) Developmental morphology of calcium oxalate foreign body stones in rats. *Calcif Tissue Int* 37: 165–173 [PubMed: 3924373]
- [18]. Khan SR, Hackett RL (1987) Urolithogenesis of mixed foreign body stones. *J Urol* 138: 1321–1328 [PubMed: 3312647]
- [19]. VERMEULEN CW, GROVE WJ, GOETZ R, RAGINS HD, CORRELL NO (1950) Experimental urolithiasis. I. Development of calculi upon foreign bodies surgically introduced into bladders of rats. *J Urol* 64: 541–548 [PubMed: 14779366]
- [20]. Chidambaram A, Rodriguez D, Khan S, Gower L (2015) Biomimetic Randall’s plaque as an in vitro model system for studying the role of acidic biopolymers in idiopathic stone formation. *Urolithiasis* 43 Suppl 1: 77–92
- [21]. Gower LB (2008) Biomimetic model systems for investigating the amorphous precursor pathway and its role in biomineralization. *Chem Rev* 108: 4551–4627 [PubMed: 19006398]
- [22]. Gower L, Odom D (2000) Deposition of calcium carbonate films by a polymer-induced liquid-precursor (PILP) process. *Journal of Crystal Growth* 210: 719–734
- [23]. Wolf SE, Harris J, Lovett A, Gower L (2017) Non-Classical Crystallization Processes: Potential Relevance to Stone Formation In: Coe F, Worcester EM, Lingeman JE, Evan AP (eds) *Kidney Stones: Medical and Surgical Management*. Jaypee Brothers, Medical Publishers Pvt. Limited, Philadelphia, PA
- [24]. Amos FF, Dai L, Kumar R, Khan SR, Gower LB (2009) Mechanism of formation of concentrically laminated spherules: implication to Randall’s plaque and stone formation. *Urol Res* 37: 11–17 [PubMed: 19066874]
- [25]. Amos FF, Olszta MJ, Khan SR, Gower LB (2006) Relevance of a Polymer-Induced Liquid-Precursor (PILP) Mineralization Process to Normal and Pathological Biomineralization In: Königsberger E, Königsberger L (eds) *Biomineralization- Medical Aspects of Solubility*. John Wiley & Sons, Ltd, West Sussex, England, pp 125–127
- [26]. Gower LB, Amos FF, Khan SR (2010) Mineralogical signatures of stone formation mechanisms. *Urol Res* 38: 281–292 [PubMed: 20625894]
- [27]. Lovett AC, Khan SR, Gower LB (2018) Development of a two-stage in vitro model system to investigate the mineralization mechanisms involved in idiopathic stone formation: stage 1—biomimetic Randall’s plaque using decellularized porcine kidneys. *Urolithiasis Online*: 10.1007/s00240-00018-01060-z
- [28]. Ross EA, Williams MJ, Hamazaki T, et al. (2009) Embryonic stem cells proliferate and differentiate when seeded into kidney scaffolds. *J Am Soc Nephrol* 20: 2338–2347 [PubMed: 19729441]
- [29]. Khan SR, Hackett RL (1986) Identification of urinary stone and sediment crystals by scanning electron microscopy and x-ray microanalysis. *J Urol* 135: 818–825 [PubMed: 3959214]
- [30]. Graeser S, Postl W, Bojar H-P, et al. (2008) Struvite-(K),  $\text{KMgPO}_4 \cdot 6\text{H}_2\text{O}$ , the potassium equivalent of struvite—a new mineral. *European Journal of Mineralogy* 20: 629–633
- [31]. Wilsenach JA, Schuurbiens CA, van Loosdrecht MC (2007) Phosphate and potassium recovery from source separated urine through struvite precipitation. *Water Res* 41: 458–466 [PubMed: 17126877]

- [32]. Khan SR, Finlayson B, Hackett RL (1983) Experimental induction of crystalluria in rats using mini-osmotic pumps. *Urol Res* 11: 199–205 [PubMed: 6659210]
- [33]. Khan SR, Glenton PA (1995) Deposition of calcium phosphate and calcium oxalate crystals in the kidneys. *J Urol* 153: 811–817 [PubMed: 7861545]
- [34]. Parks JH, Coe FL, Evan AP, Worcester EM (2009) Urine pH in renal calcium stone formers who do and do not increase stone phosphate content with time. *Nephrol Dial Transplant* 24: 130–136 [PubMed: 18662977]
- [35]. Hallson PC, Rose GA (1989) Measurement of calcium phosphate crystalluria: influence of pH and osmolality and invariable presence of oxalate. *Br J Urol* 64: 458–462 [PubMed: 2611613]
- [36]. Spradling K, Vernez SL, Khoylar C, et al. (2016) Prevalence of Hyperoxaluria in Urinary Stone Formers: Chronological and Geographical Trends and a Literature Review. *J Endourol* 30: 469–475 [PubMed: 26738689]
- [37]. Daudon M, Letavernier E, Frochot V, Haymann J-P, Bazin D, Jungers P (2016) Respective influence of calcium and oxalate urine concentration on the formation of calcium oxalate monohydrate or dihydrate crystals. *Comptes Rendus Chimie* 19: 1504–1513
- [38]. Wesson JA, Worcester E (1996) Formation of hydrated calcium oxalates in the presence of poly-L-aspartic acid. *Scanning Microsc* 10: 415–423; 423–414 [PubMed: 9813620]
- [39]. Sethmann I, Wendt-Nordahl G, Knoll T, Enzmann F, Simon L, Kleebe HJ (2017) Microstructures of Randall’s plaques and their interfaces with calcium oxalate monohydrate kidney stones reflect underlying mineral precipitation mechanisms. *Urolithiasis* 45: 235–248 [PubMed: 27695926]
- [40]. Khan SR (2004) Crystal-induced inflammation of the kidneys: results from human studies, animal models, and tissue-culture studies. *Clin Exp Nephrol* 8: 75–88 [PubMed: 15235923]
- [41]. Grases F, Costa-Bauza A, Gomila I, Conte A (2010) Origin and types of calcium oxalate monohydrate papillary renal calculi. *Urology* 76: 1339–1345 [PubMed: 20466410]
- [42]. Frochot V, Daudon M (2016) Clinical value of crystalluria and quantitative morphoconstitutional analysis of urinary calculi. *Int J Surg* 36: 624–632 [PubMed: 27847293]

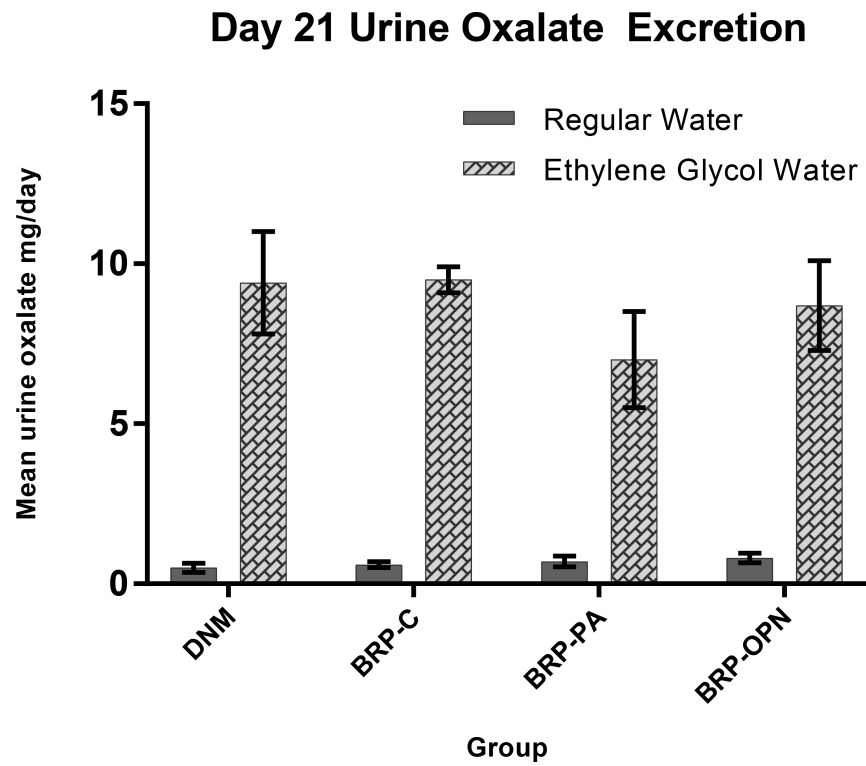


**Fig. 1.** Mean 24-hour urinary oxalate excretion at Day 21. Error bars indicated standard deviation. DNM (decellularized non-mineralized group); BRP-C (biomimetic Randall's plaque-conventionally mineralized group); BRP-PA (biomimetic Randall's plaque with polyaspartic acid group); BRP-OPN (biomimetic Randall's plaque with osteopontin group); R=regular water; EG= ethylene glycol water



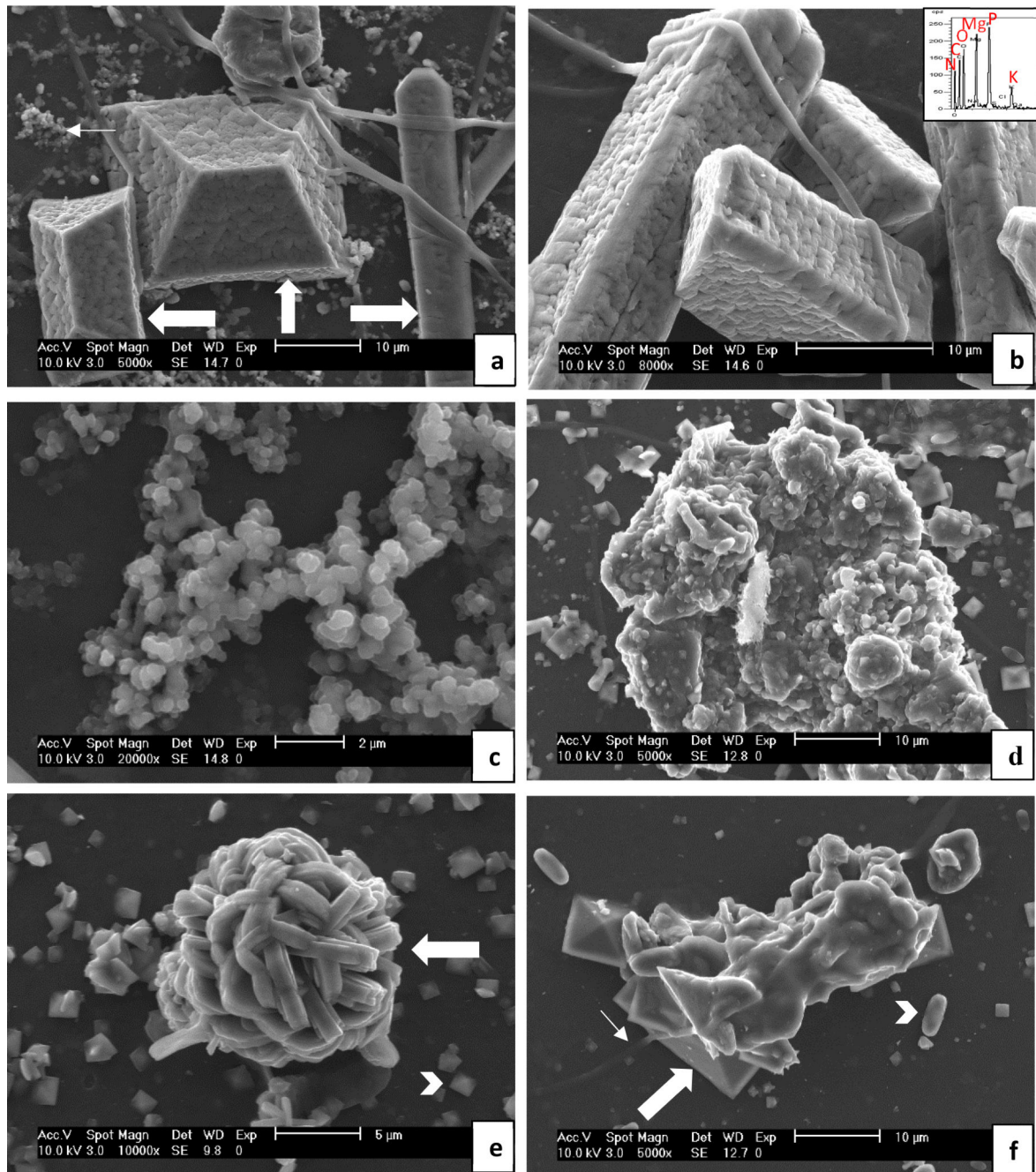


**Fig. 2.** Representative SEM images of crystals extracted from rat urine. The group the crystals were extracted from is indicated in parentheses, but similar features were observed for all the regular water (a – c) or all the ethylene glycol water (d – e) groups. (a & b) Large struvite crystals were prevalent (thick arrows). EDS (inset) shows the expected peaks for struvite of N, Mg, P, O, along with K, which occurs in the potassium magnesium phosphate form ( $\text{KMg}(\text{PO}_4)\cdot 6\text{H}_2\text{O}$ ), as well as C (presumably from organic matter). The crystals were well faceted, but had a rough surface texture that appears to be a coating of some sort, as evidenced by the cracks that can be seen in the coating (such as just above the arrow on the



right, vertically oriented crystal). There are small clusters of amorphous mineral or organic granules in background (thin arrow), similar to those seen in the higher mag. image of (c), which seem to suggest that these amorphous particles (possibly formed during drying) attached to form the coating on the large crystals (BRP-C). (c) Clusters of granular precipitates with non-descript morphologies, suggesting they were or may still be amorphous at this point (BRP-C). (d) Large granular precipitate. Fragments of BRPs were occasionally observed in the urine that seemed to have dislodged from the implants, so these may be from such fragments, or they may have created favorable substrates for continued mineral accumulation (BRP-OPN). (e) Spherical cluster of COM crystals which appear to be heavily twinned (thick arrow), along with a multitude of small COD crystals (arrow head) in background (BRP-DNM). (f) Agglomerate of COD crystals (thick arrow) containing some smooth and non-descript material, alongside smaller COD and COM (arrowhead) crystals in background. The fibrous strand (thin arrow) suggests this agglomerate originated from some dislodged implant material (BRP-PA). Scale bars are as follows: (a) 10  $\mu\text{m}$ , (b) 10  $\mu\text{m}$ , (c) 2  $\mu\text{m}$ , (d) 10  $\mu\text{m}$ , (e) 5  $\mu\text{m}$ , (f) 10  $\mu\text{m}$

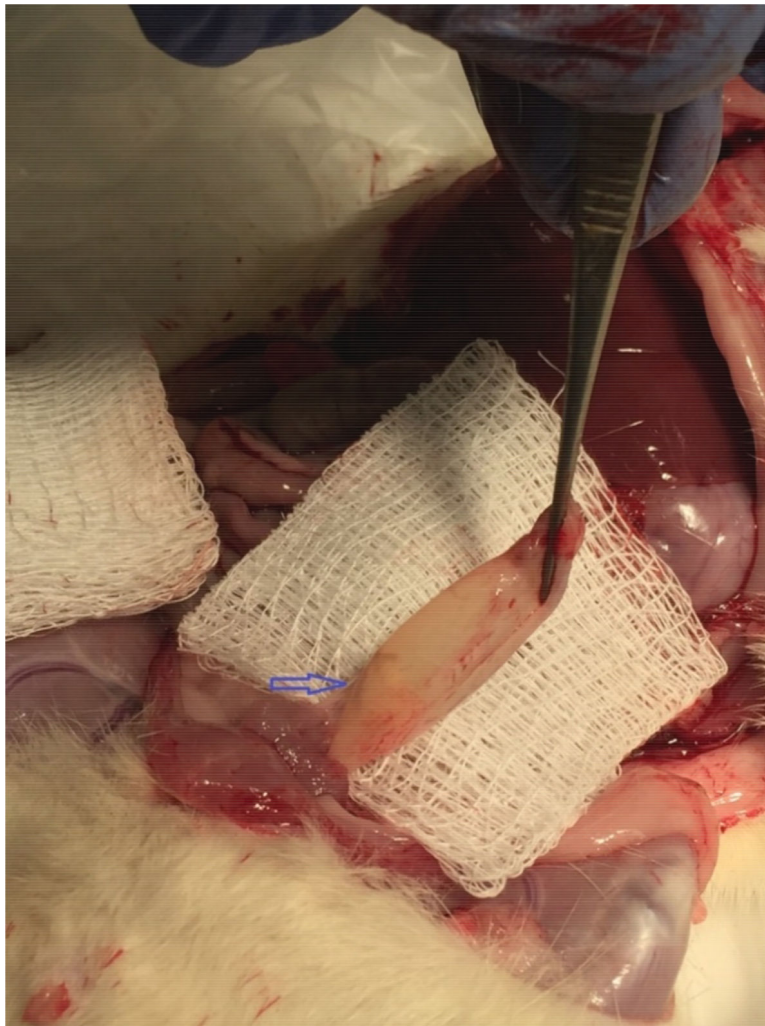


**Fig. 3.** Gross post-mortem image of rat bladder *in-situ* with intraluminal BRP at bladder apex (arrow). The bladder has been transected at the urethra and is being grasped with forceps at the level of previous urethral attachment. The image was acquired during post-mortem removal of the bladder.

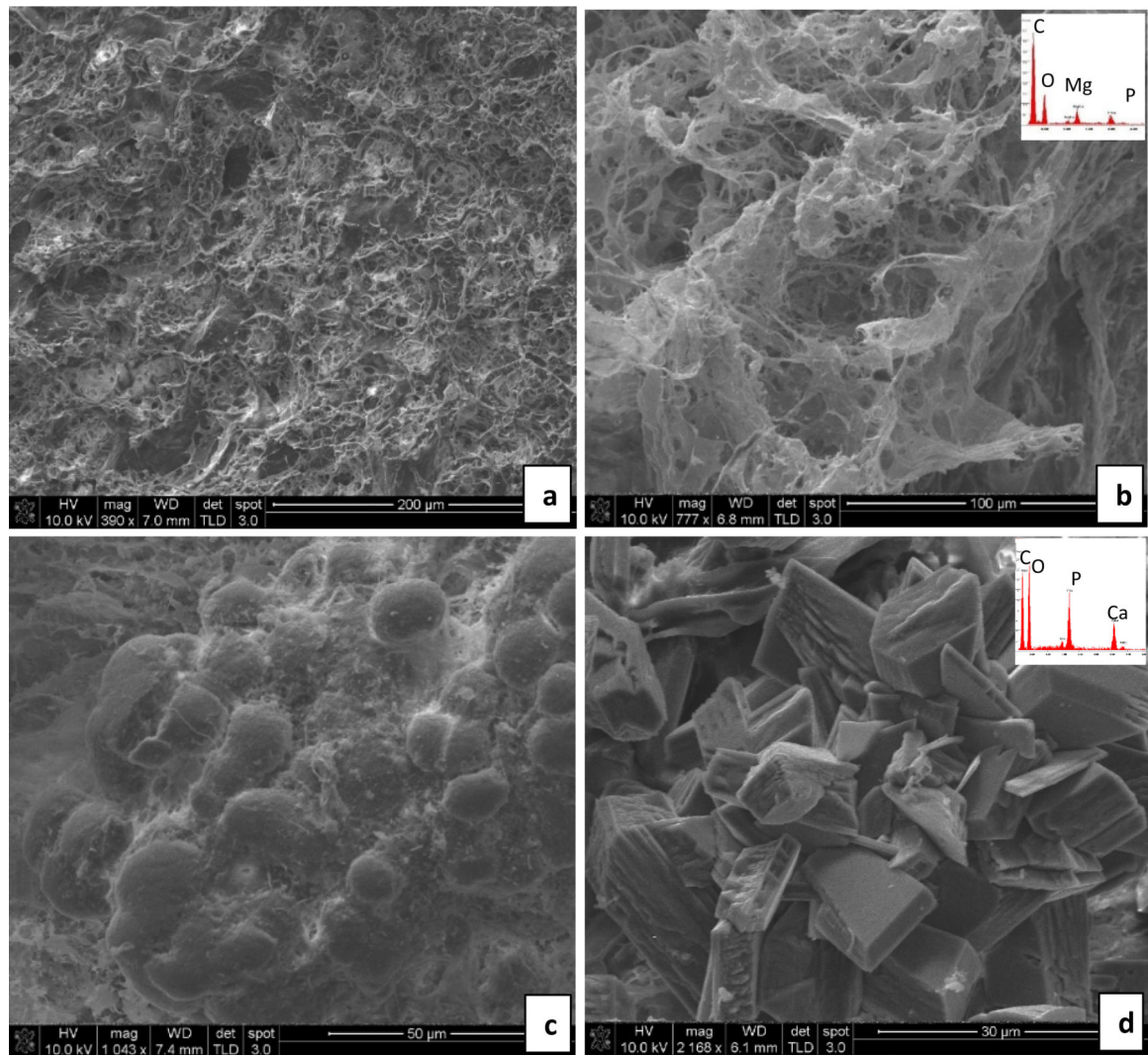


**Fig. 4.** Representative SEM images and energy dispersive spectroscopy (EDS) spectra (insets) obtained from stones overgrown on the implants– Regular water group. (a & b) DNM group: In (a), the tissue matrix contains a small amount of magnesium phosphate mineral without visibly obvious crystals, even though the EDS spectrum (b inset) detects these elements. (c & d) BRP-C group: In (c), a calcium phosphate spherulitic coating is comprised of fine crystals, probably those of the original BRP but with an accumulation of some organic debris. In (d), very large calcium phosphate crystals, unlike the morphology of the crystals in the original BRP, have formed. Scale bars are as follows: (a) 200  $\mu$ m, (b) 100  $\mu$ m, (c) 50  $\mu$ m, (d) 30  $\mu$ m

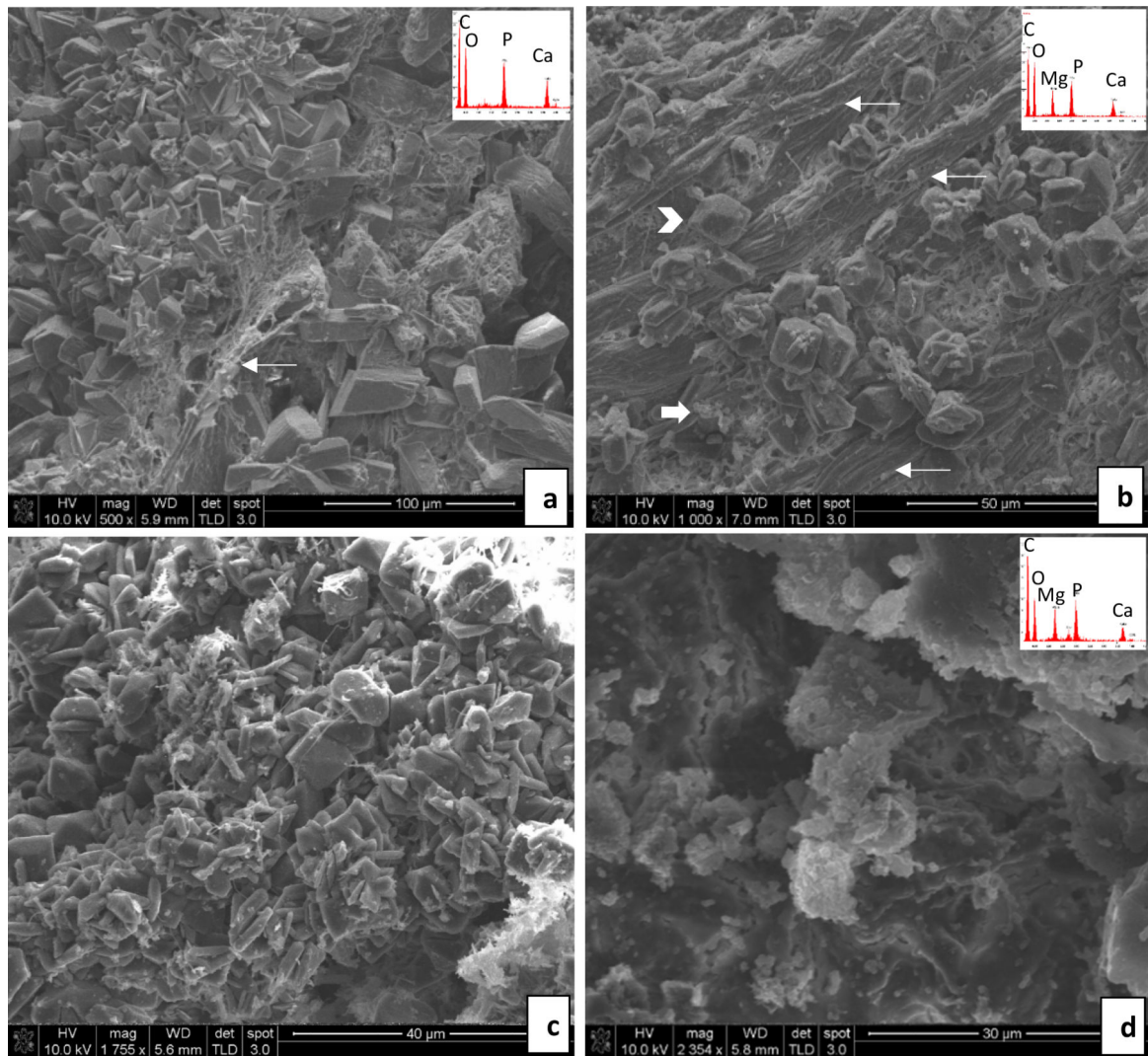


**Fig. 5.** Representative SEM images and energy dispersive spectroscopy (EDS) spectra (insets) obtained from stones overgrown on implants– Regular water group. (a & b) BRP-PA group: In (a), large calcium phosphate crystals are randomly organized amongst a fibrous segment of BRP tissue (thin arrow). In (b), multiple BRP tissue fibers are visible (thin arrows) amidst magnesium phosphate (arrow head) and granular precipitates (thick arrow). (c & d) BRP-OPN group: In (c), a high density of magnesium phosphate (struvite type) crystals. In (d), a crust of poorly defined, granular agglomerates of calcium phosphate and magnesium phosphate crystals or amorphous mineral. Scale bars are as follows: (a) 100  $\mu\text{m}$ , (b) 50  $\mu\text{m}$ , (c) 40  $\mu\text{m}$ , (d) 30  $\mu\text{m}$



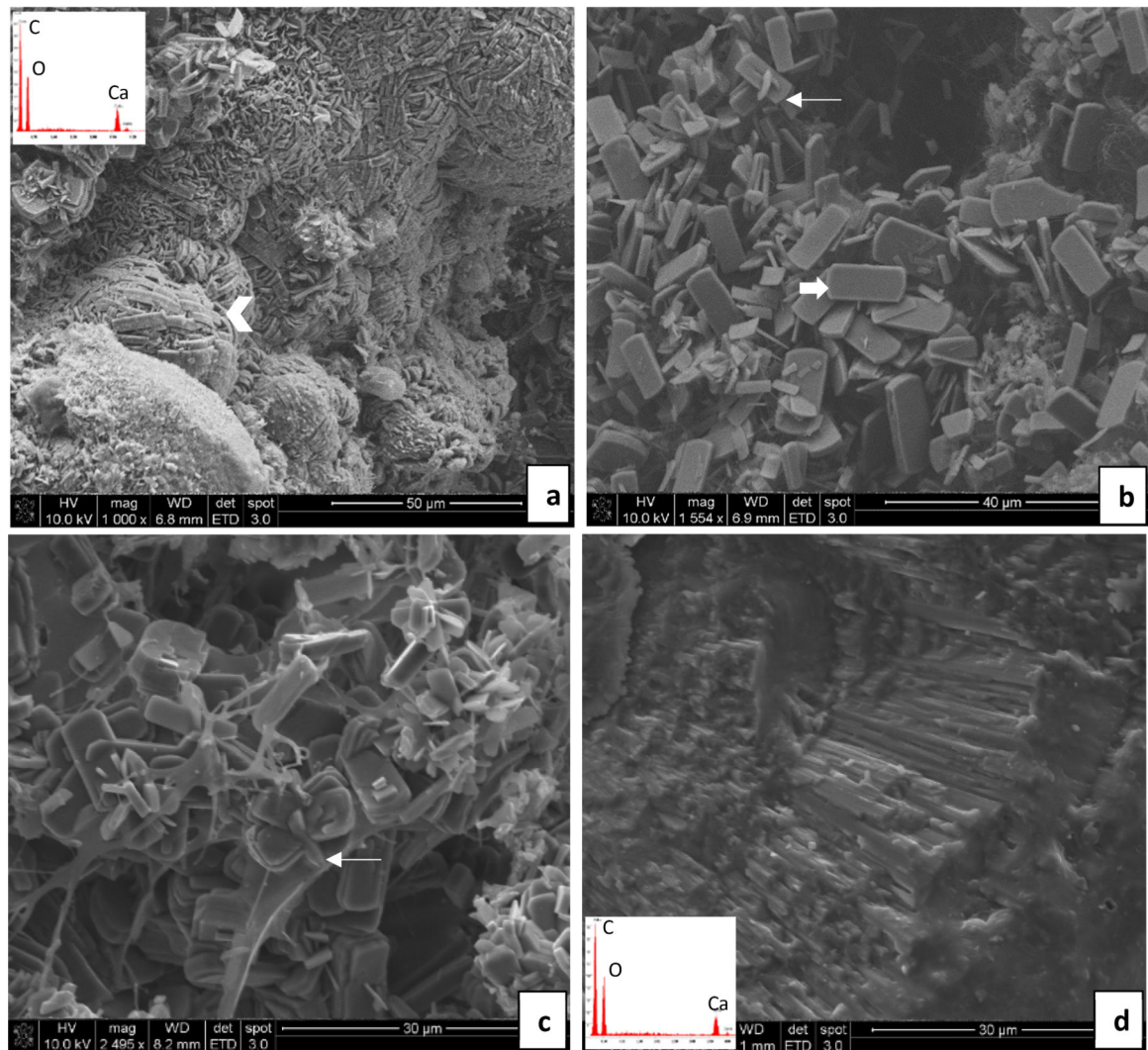


**Fig. 6.** Representative SEM images and energy dispersive spectroscopy (EDS) spectra (insets) obtained from stones overgrown on implants – ethylene glycol water group. (a & b) DNM group: In (a), densely-packed calcium oxalate monohydrate (COM) crystals (arrowhead) are organized into compact aggregates resembling those seen in stones. In (b), a random collection of tablet or plate-like COM crystals (thick arrow) are visible, with occasional interpenetrant twinning (thin arrow). (c & d) BRP-C group: In (c), conventional (faceted) COM crystals with tablet-like morphologies are seen, many that have formed clusters that likely arise from interpenetrant twinning (thin arrow). In (d), stone fragment is comprised of densely-packed radial striations, as occurs in spherulites, and which appears to have fractured at layers containing organic matrix. Scale bars are as follows: (a) 50  $\mu\text{m}$ , (b) 40  $\mu\text{m}$ , (c) 30  $\mu\text{m}$ , (d) 30  $\mu\text{m}$

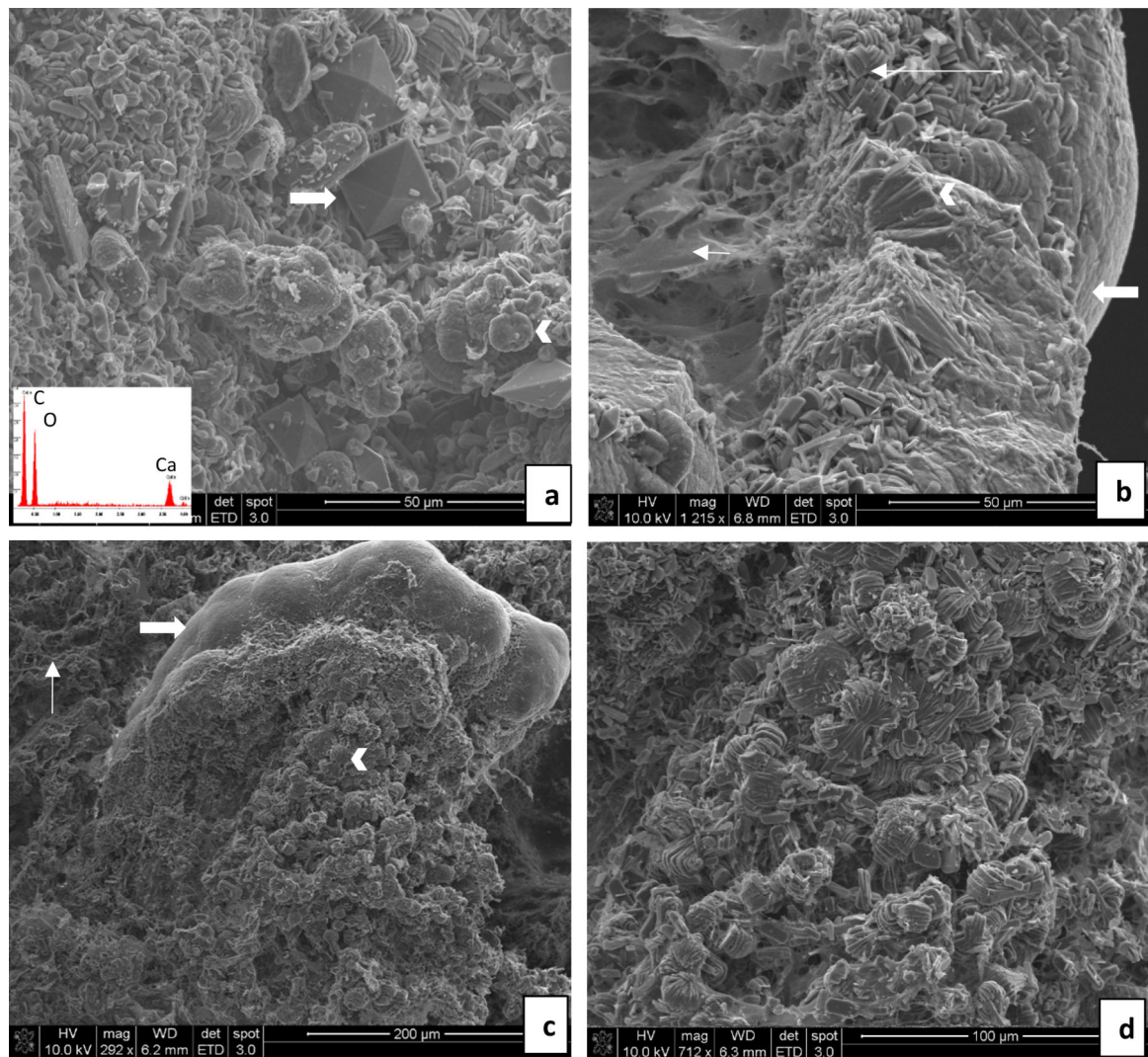


**Fig. 7.** Representative SEM images and energy dispersive spectroscopy (EDS) spectra (insets) obtained from stones overgrown on implants – ethylene glycol water group. (a & b) BRP-PA group: Agglomerates of calcium oxalate crystals covered the implant. In (a), calcium oxalate monohydrate (COM) crystals are prevalent, many of which are loose and random, while some are layered and in dumbbell form (arrowhead). A few large calcium oxalate dihydrate (COD) crystals are present and have adopted the common habit of tetragonal bipyramid (thick arrow). In (b), the surface of the stone is compact (thick arrow), as might occur on the surface of a spherulite. Although some regions are comprised of radially arranged crystals as expected for a spherulite (arrowhead), other regions consist of less organized but densely stacked (long arrow) COM crystals. BRP organic matrix is also visible toward the interior (short arrow). (c & d) BRP-OPN group: In (c), one region consists of a compact calcium oxalate stone surface morphology (thick arrow), with more faceted COM crystals being visible internally, often forming dumbbells (arrowhead). BRP fibers are also visible (thin arrow). At higher magnification in (d), the dumbbells are seen to be



comprised of stacked aggregates of thickly layered COM tablets. Scale bars are as follows:  
(a) 50  $\mu\text{m}$ , (b) 50  $\mu\text{m}$ , (c) 200  $\mu\text{m}$ , (d) 100  $\mu\text{m}$

Author Manuscript

Author Manuscript

Author Manuscript

Author Manuscript